Influence of the Structure on the Electrochemical Performance of Lithium Transition Metal Phosphates as Cathodic Materials in Rechargeable Lithium Batteries: A New High-Pressure Form of $LiMPO_4$ (M = Fe and Ni)

O. García-Moreno,[†] M. Alvarez-Vega,[†] F. García-Alvarado,[†] J. García-Jaca,[‡] J. M. Gallardo-Amores,[‡] M. L. Sanjuán,[§] and U. Amador*,[†]

Departamento de Química Inorgánica y Materiales, Facultad de Ciencias Experimentales y Técnicas, Universidad San Pablo-CEU, Urbanización Montepríncipe, 28668 Boadilla del Monte, Madrid, Spain, Laboratorio de Altas Presiones, Facultad de Ciencias Químicas, Universidad Complutense, 28040 Madrid, Spain, and Instituto de Ciencia de Materiales de Aragón, Universidad de Zaragoza-CSIC, Facultad de Ciencias, 50009 Zaragoza, Spain

Received July 24, 2000. Revised Manuscript Received February 6, 2001

Materials built from MO_6 octahedra linked to XO_4 tetrahedra are good candidates for studying the different factors that determine the electrode potential. Among them, olivine-like $LiMPO_4$ (M = transition metal) phosphates are especially interesting. When pressure is applied to $LiMPO_4$ (M = Ni and Fe), a phase transition is induced. However, instead of the well-known olivine ⇔ spinel transformation, a transition to a new phase is observed (β'). The arrangements of the metal ions (including phosphorus) in the two structures are very similar; thus, the main difference between them is due to the oxygen arrangement in a similar matrix. Raman spectroscopy has confirmed the structural model proposed for the high-pressure phase, in particular the modification in the lithium coordination from 6- to 4-fold upon synthesis under pressure. Among the olivines $LiMPO_4$ (M = Mn, Ni, and Fe), the iron-containing one is only active up to 5.1 V. On the other hand, none of the high-pressure materials is electrochemically active; this can be explained by the change in the electrostatic field at the transition metal position.

Introduction

During the past few years the search for new cathode materials for rechargeable lithium batteries has been mainly focused on lithium transition metal oxides. Among them, the most useful or promising are those with a layered rock-salt structure or spinel-like structure.[1−6] The latter compounds show the highest voltage of a working redox couple found so far;[5,6] high oxidation voltage is necessary to obtain high specific energy in a battery constructed with a given anode. Thus, in the design of new cathodic materials, an understanding of the chemical and the structural features that control the energy of the active redox couple, and as a consequence the voltage, is of crucial importance. The energy of a given redox couple varies from one material to another depending on two main factors: (1) the electrostatic field at the cation position and (2) the covalent contribution to the cation−anion bonding. The study of both factors can be properly accomplished on oxides formed by MO_6 octahedra (M = transition metal cation) linked by tetrahedral polyanions (XO_4^{n-} = PO_4^{3-}, AsO_4^{3-}, SO_4^{2-}, MoO_4^{2-}, etc.). The electrostatic field changes when the structure does, whereas the covalence of the M−O bond differs in isostructural compounds with different tetrahedral polyanions by inductive effect due to the different degrees of covalence in the X−O bond.[7] Among the above compounds, olivine-like phosphates are extremely interesting, not only from a basic point of view, but also for their possible use as cathodic materials. In this connection, $LiCoPO_4$ olivine has very recently been reported to be a high-voltage/high-energy electrode.[8]

In addition to the preparation of a new form of $LiMPO_4$ (M = Fe and Ni) materials obtained under high pressure from the corresponding olivine-like compounds and the characterization of the two structures by Raman spectroscopy, in this paper, the electrochemical behavior of both series of compounds is presented and discussed in connection with their structures.

* Corresponding author. Telephone: 34 91 372 47 37. Fax: 34 91 351 04 75. E-mail: uamador@ceu.es.
[†] Universidad San Pablo-CEU.
[‡] Universidad Complutense.
[§] Universidad de Zaragoza-CSIC.

(1) Broussely, M. *J. Power Sources* **1999**, *81−82*, 137.
(2) Broussely, M. *J. Power Sources* **1999**, *81−82*, 140.
(3) Kodama, T.; Sakaebe, H. *J. Power Sources* **1999**, *81−82*, 144.
(4) Owens, B. B.; Smyrl, W. H.; Xu, J. J. *J. Power Sources* **1999**, *81−82*, 150.
(5) Kawai, H.; Nagata, M.; Tsukamoto, H.; West, A. R. *Electrochem. Solid-State Lett.* **1998**, *1*, 212.
(6) Fey, G.; Li, W.; Dand, J. R. *J. Electrochem. Soc.* **1994**, *141*, 2279.
(7) Padhi, A. K.; Nanjundaswamy, K. S.; Goodenough, J. B. *J. Electrochem. Soc.* **1997**, *144*, 1188.
(8) Amine, K.; Yasuda, K.; Yamachi, M. *Electrochem. Solid-State Lett.* **2000**, *3* (4), 178.

10.1021/cm000596p CCC: $20.00
Published on Web 04/13/2001

Table 1. Final Structural Parameters of $LiMPO_4$ Olivine-like Compounds

			M = Mn[a]				M = Fe[b]				M = Ni[c]			
atom	site	symm[d]	*x/a*	*y/b*	*z/c*	B_{iso} (Å^2)	*x/a*	*y/b*	*z/c*	B_{iso} (Å^2)	*x/a*	*y/b*	*z/c*	B_{iso} (Å^2)
Li	4a	−1	0	0	0	1.7(5)	0	0	0	1.1(4)	0	0	0	0.69(2)
M	4c	.*m*.	0.2826(5)	1/4	0.972(1)	0.6(2)	0.2857(5)	1/4	0.9737(8)	0.8(2)	0.2760(3)	1/4	0.9809(7)	0.37(2)
P	4c	.*m*.	0.096(1)	1/4	0.413(1)	0.5(2)	0.0943(7)	1/4	0.4265(5)	0.4(1)	0.0945(6)	1/4	0.420(1)	0.37(2)
O(1)	4c	.*m*.	0.099(2)	1/4	0.732(5)	0.8(3)	0.094(3)	1/4	0.746(1)	0.9(3)	0.092(1)	1/4	0.745(2)	0.21(1)
O(2)	4c	.*m*.	0.456(2)	1/4	0.216(3)	0.8(3)	0.451(1)	1/4	0.193(2)	0.9(3)	0.450(1)	1/4	0.219(2)	0.21(1)
O(3)	8d	1	0.157(1)	0.047(3)	0.274(2)	0.8(3)	0.167(1)	0.050(3)	0.300(2)	0.9(3)	0.1624(9)	0.045(1)	0.276(2)	0.21(1)

[a] For M = Mn, a = 10.431(9) Å, b = 6.0947(6) Å, c = 4.7366(5) Å, V = 301.12(3) Å^3, ρ = 3.46(1) g/cm^3, R_B = 0.079, R_{exp} = 0.075, R_{wp} = 0.21, χ^2 = 7.7. [b] For M = Fe, a = 10.227(1) Å, b = 6.0048(7) Å, c = 4.6918(7) Å, V = 288.12(4) Å^3, ρ = 3.88(1) g/cm^3, R_B = 0.057, R_{exp} = 0.060, R_{wp} = 0.22, χ^2 = 14. [c] For M = Ni, a = 10.0275(3) Å, b = 5.8537(2) Å, c = 4.6763(2) Å, V = 274.49(1) Å^3, ρ = 3.88(1) g/cm^3, R_B = 0.057, R_{exp} = 0.087, R_{wp} = 0.151, χ^2 = 2.95. [d] Symmetry group = *Pnma* (62).

Experimental Section

$LiMPO_4$ (M = Mn or Ni) compounds with olivine-like structures were prepared by the reaction of stoichiometric amounts of analytical-grade (Aldrich 99.99%) $M(CO_3)$, $(NH_4)_2HPO_4$ and Li_2CO_3 under flowing argon. The samples enriched with ^{6}Li used in the Raman experiments were prepared using $^6LiOH{\cdot}H_2O$ (Aldrich) as the lithium source. To obtain single-phase samples the thermal treatment was performed in three different steps: (1) 398 K for 24 h, (2) 498 K for 24 h, and (3) 1023 K for 48 h. After each treatment, the sample was ground and pelletized. To obtain a single-phase sample of the iron-containing olivine, $Fe_3(PO_4)_2$ must be used as the iron source, because, when iron carbonate or nitrate is used, some impurity phases appear. This Fe(II) phosphate was prepared by direct reaction of $FePO_4$ and metallic iron in an evacuated quartz ampule at 1073 K for 24 h. Following the above procedure, pale orange, strong yellow, and gray samples were obtained for manganese, nickel, and iron, respectively.

The high-pressure experiments were performed on a belt-type press working at 65 kbar and 1173 K. In all cases, the high-pressure materials had a pale green color.

The samples were determined to be single-phase by X-ray powder diffraction with a Siemens D501 apparatus using monochromatic Cu Kα radiation. The X-ray diffraction data were analyzed using the program Fullprof.[9]

Thermal analyses were carried out to assess the chemical stability of the single-phase samples up to 872 °C on a Seiko 320U system. Experiments were run at heating rate of 10 °C min^{-1} (Pt/Pt−Rh thermocouple) in a dry air stream flowing at 100 mL min^{-1} (typical specimen weight of 10−12 mg).

The Raman spectra were measured at room temperature in a Dilor XY spectrometer with a diode-array multichannel detector. Light from a Coherent Ar$^+$ laser at 514.5 nm was focused onto the sample through a ×50 microscope objective lens. The light power at the sample was 10 mW, and the spot size was 4 μm^2. The spectral resolution was typically 3 cm^{-1}.

The lithium ionic conductivity was measured on pellets of the samples by ac impedance spectroscopy using a Solartron 160 impedance analyzer over a frequency range from 20 Hz to 20 MHz and a temperature range from room temperature to 772 K. Both opposite faces of the pellets were pasted with platinum electrodes.

The electrochemical experiments were performed in Swagelok cells with the following configuration: Li/$LiPF_6$ (1 M) in EC (ethylene carbonate) + DMC (dimethyl carbonate) (1:1)/host material + carbon black + binder. Cells were cycled under potentiostatic conditions using ±10 mV/0.5 h steps; the cell voltage was measured against the lithium metal electrode.

Results and Discussions

Structural Study. From powder X-ray diffraction experiments, the samples $LiMPO_4$ (M = Mn, Fe and Ni) were found to be single-phase with an olivine-like structure. Figure 1 shows the result of fitting the experimental X-ray diffraction pattern for $LiNiPO_4$ using as starting model the structure proposed in ref 10; the difference between the observed and calculated data is also shown. The patterns corresponding to the other $LiMPO_4$ olivine-like materials are similar. The final structural parameters for all compounds are collected in Table 1, and Table 2 shows some selected interatomic distances. In Figure 2a, a schematic representation of the olivine structure is depicted. This structure is usually described in terms of a hexagonal close-packing of oxygen with Li and M ions located in one-half of the octahedral sites and P in one-eighth of the tetrahedral positions. The MO_6 octahedra share four corners in the *cb* plane being cross-linked along the *a* axis by the PO_4 groups, whereas the Li ions are located in rows, running along *a*, of edge-shared LiO_6 octahedra that appear between two consecutive $[MO_6]_\infty$ layers described above.[11]

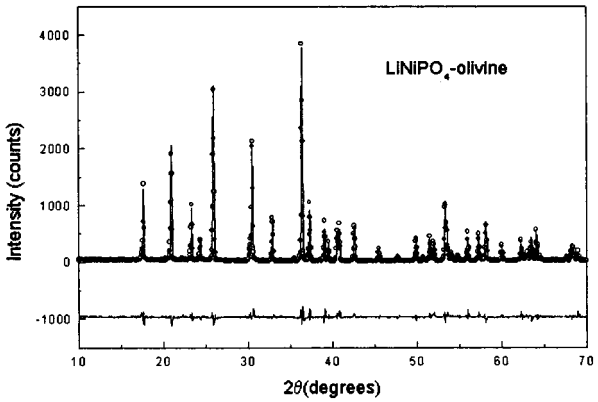

Figure 1. Results of fitting the X-ray powder diffraction data corresponding to olivine $LiNiPO_4$: experimental (points), calculated (solid line), and difference (bottom).

Table 2. Selected Interatomic Distances in Olivine-like $LiMPO_4$ Compounds

M = Mn		M = Fe		M = Ni	
Mn−O(1)	2.23(1)	Fe−O(1)	2.25(1)	Ni−O(1)	2.15(1)
Mn−O(2)	2.14(2)	Fe−O(2)	2.00(1)	Ni−O(2)	2.07(1)
Mn−O(3)	2.13(2) × 2	Fe−O(3)	2.03(1) × 2	Ni−O(3)	2.072(8) × 2
Mn−O(3)	2.30(2) × 2	Fe−O(3)	2.30(1) × 2	Ni−O(3)	2.150(8) × 2
P−O(1)	1.50(3)	P−O(1)	1.50(1)	P−O(1)	1.52(1)
P−O(2)	1.59(3)	P−O(2)	1.58(1)	P−O(2)	1.59(2)
P−O(3)	1.54(2) × 2	P−O(3)	1.53(1) × 2	P−O(3)	1.540(9) × 2
Li−O(1)	2.24(2) × 2	Li−O(1)	2.15(1) × 2	Li−O(1)	2.101(8) × 2
Li−O(2)	2.08(1) × 2	Li−O(2)	2.14(1) × 2	Li−O(2)	2.030(8) × 2
LI−O(3)	2.11(1) × 2	LI−O(3)	2.25(1) × 2	LI−O(3)	2.090(8) × 2

(9) Rodríguez-Carvajal, J. FULLPROF, version 2.4.2; ILL (unpublished).

(10) Abrahams, I.; Durand, J. L. *Acta Crystallogr. C* **1993**, *49*, 925.
(11) Megaw, H. D. *Crystal Structures: A Working Approach*; Saunders: London, 1973.

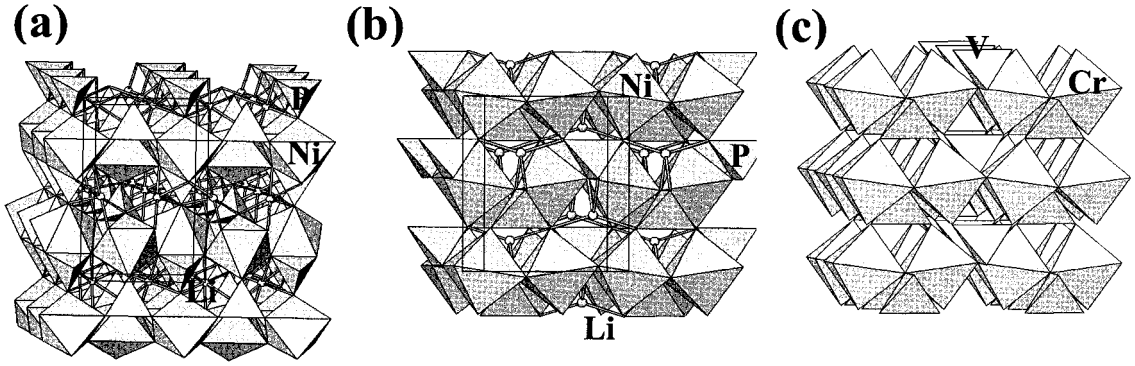

Figure 2. Schematic representation of the structures of (a) olivine, (b) β'-$LiNiPO_4$, and (c) $CrVO_4$.

Table 3. Final Structural Parameters of β'-$LiMPO_4$ Compounds

			M = Fe[a]				M = Ni[b]			
atom	site	symmetry[c]	*x*/*a*	*y*/*b*	*z*/*c*	B_{iso} (Å^2)	*x*/*a*	*y*/*b*	*z*/*c*	B_{iso} (Å^2)
Li	4c	*m*2*m*	0	0.676(2)	1/4	1.8(6)	0	0.675(2)	1/4	1.5(6)
M	4a	2/*m*..	0	0	0	1.0(3)	0	0	0	0.54(4)
P	4c	*m*2*m*	0	0.3504(6)	1/4	1.2(4)	0	0.3504(3)	1/4	0.62(4)
O(1)	8f	*m*..	0	0.247(1)	0.043(1)	1.5(5)	0	0.246(3)	0.044(1)	0.87(5)
O(2)	8g	..*m*	0.228(1)	0.467(1)	1/4	1.5(5)	0.227(1)	0.466(3)	1/4	0.87(5)

[a] For M = Fe, a = 5.5230(3) Å, b = 8.2565(5) Å, c = 6.1583(3) Å, V = 280.82(5) Å^3, ρ = 3.73(2) g/cm^3, R_B = 0.055, R_{exp} = 0.057, R_{wp} = 0.25, χ^2 = 19. [b] For M = Ni, a = 5.3580(2) Å, b = 8.1272(3) Å, c = 6.1241(3) Å, V = 266.7(1) Å^3, ρ = 4.00(2) g/cm^3, R_B = 0.033, R_{exp} = 0.028, R_{wp} = 0.09, χ^2 = 5.7. [c] Symmetry group = *Cmcm* (63).

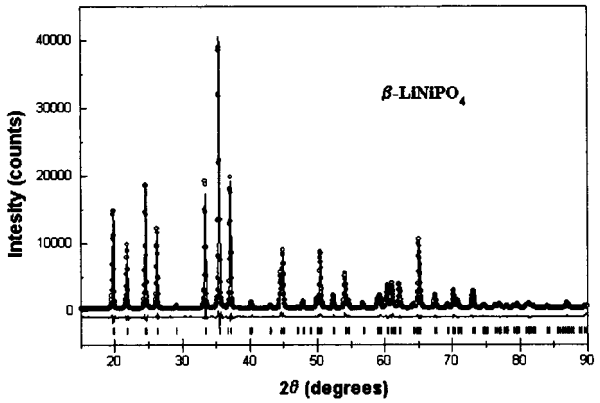

Figure 3. Experimental (points), calculated (solid line), and difference (bottom) X-ray powder diffraction patterns for β'-$LiNiPO_4$.

When pressure is applied to the $LiMPO_4$ (M = Fe and Ni) olivine-like compounds, a phase transition is induced, whereas the manganese-containing olivine seems to be stable up to the limit of the experimental setup (65 kbar). However, instead of the well-known olivine ⇔ spinel transformation,[12,13] a transition to a new phase is observed. The structure of this phase (called β'-$LiMPO_4$ hereafter), as determined by powder XRD is shown in Figure 2b. It is similar to that of $CrVO_4$ (Figure 2c),[14] with lithium ions located in empty tetrahedral positions. In Figure 3 the experimental X-ray diffraction data for β'-$LiNiPO_4$, the calculated pattern using the structural model proposed in Table 3 and their difference are shown. The pattern corresponding to β'-$LiFePO_4$ is similar to that for β'-$LiNiPO_4$. The final structural parameters for both compounds are also collected in Table 3, and Table 4 shows some selected interatomic distances.

Table 4. Selected Interatomic Distances in β'-$LiMPO_4$ Compounds

M = Fe		M = Ni	
Fe−O(1)	2.06(1) × 2	Ni−O(1)	2.03(1) × 2
Fe−O(2)	2.17(1) × 4	Ni−O(2)	2.13(1) × 4
P−O(1)	1.53(1) × 2	P−O(1)	1.55(1) × 2
P−O(2)	1.59(1) × 2	P−O(2)	1.52(1) × 2
Li−O(1)	1.91(1) × 2	Li−O(1)	1.90(1) × 2
Li−O(2)	2.14(1) × 2	Li−O(2)	2.09(1) × 2

The structure of the β'-$LiMPO_4$ (M = Fe and Ni) compounds consists of rows of edge-sharing MO_6 octahedra running along *c* that are cross-linked by LiO_4 and PO_4 tetrahedra along the *a* axis, giving rise to layers of composition $[(MO_6)(LiO_4)(PO_4)]_\infty$ lying in the *ac* plane. These layers are stacked along the *b* axis with a displacement of *a*/2 (Figure 4).

Alternatively, the structure can be described by the stacking, along the [100] direction, of mixed layers composed of MO_6 octahedra and LiO_4 and PO_4 tetrahedra. In one layer, every MO_6 octahedron shares two opposite edges with neighboring MO_6 octahedra and two apical oxygen atoms with two LiO_4 and two phosphate groups. A phosphate group shares two oxygen atoms with two different MO_6 polyhedra and one edge with a LiO_4 tetrahedron; in this way, the $[MO_6]_\infty$ edge-sharing rows are linked along the [010] direction by two rows of composition $[(LiO_4)(PO_4)]_\infty$, condensed in such a way that every LiO_4 tetrahedra in one row shares one edge with a phosphate in the second row (Figure 5). These layers are stacked along the *a* axis in such a way that the largest window in one layer is blocked on both sides by an octahedron of neighboring layers. This alternative description based on the polyhedra arrangement seems to be more suitable for determining structural relationships between this structure and the olivine one, as was previously done for the olivine ⇔ spinel transition.[12,15]

(12) Hornstra, J. *J. Phys. Chem. Solids* **1960**, *15*, 311.
(13) Binns, R. A.; Davis, R. N.; Reed, S. B. J. *Nature* **1969**, *221*, 227.
(14) Frazer, B. C.; Brown, P. J. *Phys. Rev.* **1967**, *125*, 1283.

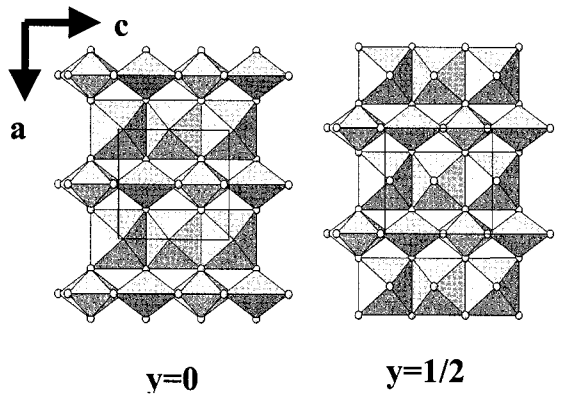

Figure 4. Schematic representation of the stacking sequence of $[(MO_6)(LiO_4)(PO_4)]_\infty$ layers along the *b* axis in β'-$LiMPO_4$ (see text).

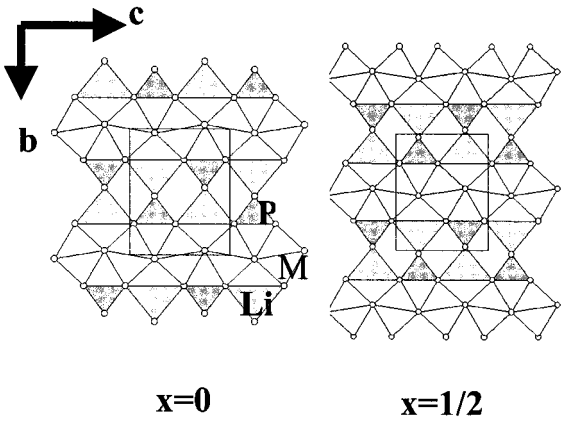

Figure 5. Depiction of the structure of β'-$LiMPO_4$ by stacking of layers along the *a* axis (see text).

In this case both olivine and spinel are close-packed structures, with a hexagonal (ABAB) sequence in the former and a cubic (ABCABC) sequence in the latter, and relationships between the two structures can be established. In contrast, the oxygen ions are not close-packed in β'-$LiMPO_4$, rendering this viewpoint less useful in describing the pressure-induced phase transition olivine ⇔ β'-$LiMPO_4$. In this connection, it is worth noting that the arrangements of metal ions (including phosphorus) in the two structures are very similar. In olivine, Ni and P define distorted hexagonal sheets stacked along the *b* axis in a hexagonal sequence (ABAB), with lithium ions located in the center of distorted octahedra of phosphorus atoms (Figure 6a). The metal framework in the β' phase is very similar, as can be seen in Figure 6b; in this case, the hexagonal sheets are formed by phosphorus and lithium, whereas the nickel ions occupy the octahedral sites defined by phosphorus. Although an important rearrangement is produced through the phase transition, the metallic frameworks in the two structures are almost the same, assuming that lithium and nickel can be interchanged. In this connection, the high-pressure phase is metastable at ambient pressure and transforms into olivine on heating (to allow for motion of the metallic ions) at about 697 K. As shown in Figure 7, when the metals

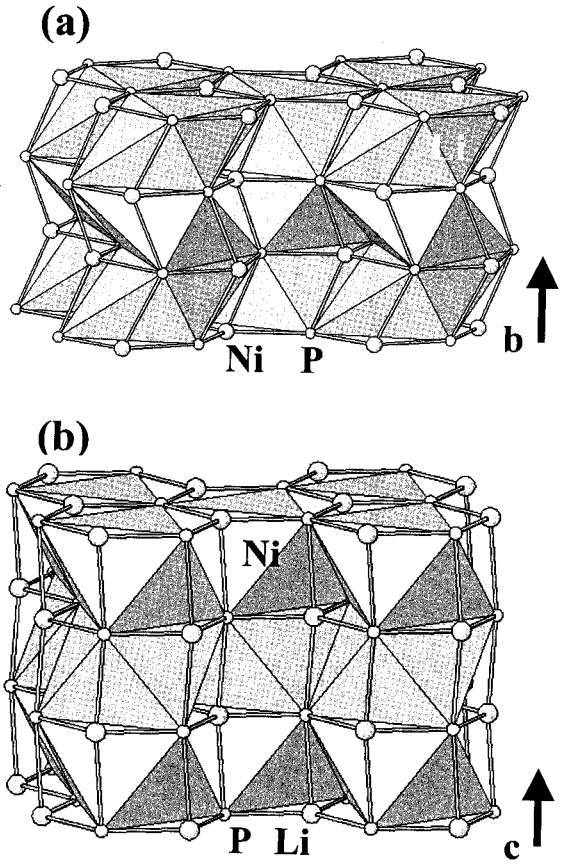

Figure 6. "Metallic" framework in (a) olivine- and (b) β'-$LiNiPO_4$.

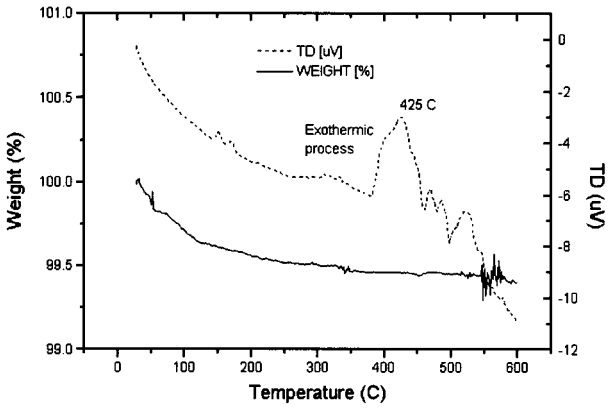

Figure 7. TGA/TDA data for β'-$LiNiPO_4$.

are rearranged, the excess energy of the β'-phase is eliminated.

It is well-known that several olivine-like compounds transform under high pressure into denser structures. Thus, the high-pressure form of the silicate Mg_2SiO_4[16] is about 6% denser than the olivine form; and some germanates, such as Ca_2GeO_4, evolve under high pressure to materials with a K_2NiF_4 structure that is about 25% denser, whereas others such as Mn_2GeO_4 transform to a Sr_2PbO_4-type structure (18% denser).[17] It is worth pointing out that the volume reduction in the transition from the olivine to the β' phase is only about 2.5%. Even more important, in general, phase transitions induced

(15) Choisnet, J.; Hervieu, M.; Raveau, B.; Tarte, P. *J. Solid State Chem.* **1982**, *45*, 280.

(16) Baur, W. H. *Am. Mineral.* **1972**, *57*, 709.
(17) Reid, A. F.; Ringwood, A. E. *J. Solid State Chem.* **1970**, *1*, 557.

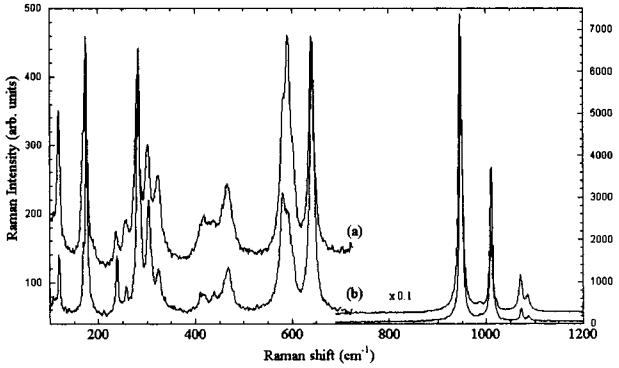

Figure 8. Raman spectra of olivine $LiNiPO_4$ with (a) natural lithium and (b) 100% ^6Li.

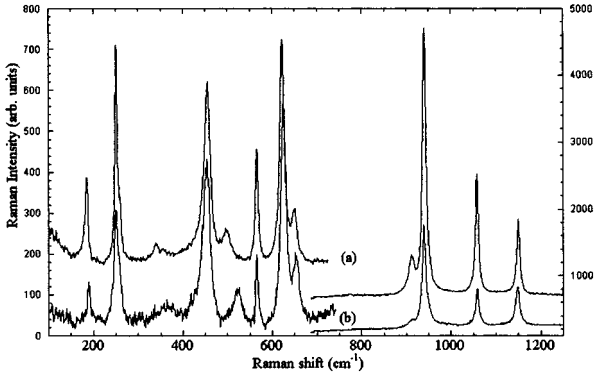

Figure 9. Raman spectra of β'-$LiNiPO_4$ with (a) natural lithium and (b) 100% ^6Li.

by pressure yield to structures with higher coordination numbers (cn's), or at least the cn's of all atoms in the low- and high-pressure phases are the same (for instance in the olivine ⇔ spinel transition). To the best of our knowledge, no pressure-induced transition has been reported so far in which the coordination number of one type of cation is lowered. This is the case in the olivine ⇔ β'-$LiMPO_4$ transition. In the olivine form of $LiMPO_4$ compounds, the lithium ions are located in the middle of edge-sharing LiO_6 octahedra. In the β'-phase, the lithium ions are located in unconnected LiO_4 tetrahedra. This description of the lithium coordination in the two structures is obtained when only the nearest oxygen atoms are considered (Li−O distances up to 2.5 Å), as is the common practice in most cases. However, if the second coordination sphere is also taken into account, the coordination of lithium increases from that of the ambient to the high-pressure structure. In particular, for Li−O distances up to 3.2 Å, the coordination numbers are 6 in olivine and 4 + 4 in the β'-phase phase. Because this is a very important point and powder XRD is not the most suitable technique for studying structural effects related to light atoms, such as lithium, a spectroscopic study was performed to confirm the proposed structural model.

Spectroscopic Study. We have measured the Raman spectrum of polycrystalline $LiNiPO_4$ in both the olivine and the β' phases. Compounds with 100% substitution of ^6Li were also studied in order to verify the assignment of some modes to lithium vibrations.

Figure 8a and b shows the Raman spectra of $LiNiPO_4$ in the olivine phase (a) with the natural proportion of lithium isotopes and (b) with 100% ^6Li. Figure 9a and b shows the corresponding spectra for the β' phase. In Figures 8 and 9, all of the resolved peaks were above 100 cm^{-1}; below this frequency, only a structureless background was found. These spectra can clearly be divided into two regions, above and below 400 cm^{-1}, that we can approximately (except for the lithium modes) correlate with the domain of appearance of internal and external modes, respectively.

Internal modes involve the displacement of oxygen atoms of the pseudo-tetrahedral $(PO_4)^{3-}$ anions and present frequencies closely related to those of the free molecule (in solution, for instance) with perfect T_d symmetry. For $(PO_4)^{3-}$, these are[18] a singlet (A_1) at a frequency $\nu_1 = 938$ cm^{-1}; a doublet (E) at $\nu_2 = 465$ cm^{-1}; and two triply degenerate (T_2) modes, ν_3 at 1027 cm^{-1} and ν_4 at 567 cm^{-1}. ν_1 and ν_3 involve the stretching of the P−O bonds, whereas ν_2 and ν_4 involve mostly O−P−O bending, with a small contribution of P vibration. In a solid, internal modes can split as a consequence of an electric crystal field of symmetry lower than tetrahedral acting on the molecule (site-symmetry effect) and also because of the presence of more than one molecular group in the crystal unit cell (correlation effect).

Table 5. Factor Group Analysis for Olivine $LiNiPO_4$

Translations of Li, Ni, PO_4: 36 modes

atom	site	A_g	A_u	B_{1g}	B_{1u}	B_{2g}	B_{2u}	B_{3g}	B_{3u}
Li	−1, 4a, C_i		3		3		3		3
Ni	.*m*., 4c, C_s^{xz}	2	1	1	2	2	1	1	2
P	.*m*., 4c, C_s^{xz}	2	1	1	2	2	1	1	2

Librations of PO_4: 12 modes

T_d	site C_s^{xz}	correlation to D_{2h}
T_1	A′ + 2A"	$A_g + B_{1u} + B_{2g} + B_{3u} + 2A_u + 2B_{1g} + 2B_{2u} + 2B_{3g}$

Internal modes of PO_4: 36 modes

T_d	site C_s^{xz}	correlation to D_{2h}
ν_1 (A_1)	A′	$A_g + B_{1u} + B_{2g} + B_{3u}$
ν_2 (E)	A′ + A"	$A_g + B_{1u} + B_{2g} + B_{3u} + A_u + B_{1g} + B_{2u} + B_{3g}$
ν_3 (T_2)	2A′ + A"	$2A_g + 2B_{1u} + 2B_{2g} + 2B_{3u} + A_u + B_{1g} + B_{2u} + B_{3g}$
ν_4 (T_2)	2A′ + A"	$2A_g + 2B_{1u} + 2B_{2g} + 2B_{3u} + A_u + B_{1g} + B_{2u} + B_{3g}$

External modes consist, on one hand, of Li, Ni, and PO_4 translations and, on the other hand, of rotational oscillations (librations) of PO_4 units. Librational modes can also show site-symmetry and correlation effects. According to this separation, factor group analysis gives the modes for $LiNiPO_4$ with the olivine structure (space group *Pnma*) collected in Table 5. Among all of these modes, only the even ones (A_g, B_{1g}, B_{2g}, B_{3g}) are Raman-active. Thus, lithium atoms located in sites with inversion symmetry are not spectroscopically active, so that we do not expect to see modes involving lithium vibrations. As a whole, we expect 12, 6, and 18 Raman modes of translational, librational, and internal character, respectively.

In the β' phase (symmetry group *Cmcm*), the activity of each type of atom is shown in Table 6. Only the 18 even modes are Raman-active, including 6 translations, 3 librations, and 9 internal modes. In this phase, lithium atoms occupy a quasi-tetrahedral site and are Raman-active. In contrast, Ni atoms, at a site of symmetry C_{2h}, are inactive.

(18) Nakamoto, K. *Infrared and Raman spectra of inorganic and coordination compounds*; J. Wiley & Sons: New York, 1978.

Table 6. Factor Group Analysis for β'-$LiNiPO_4$

Translations of Li, Ni, PO_4: 24 modes								
atom	site	A_g	A_u	B_{1g}	B_{1u}	B_{2g}	B_{2u}	B_{3u}
Li	$m2m$, 4c, C_{2v}^y	1		1	1	1	1	1
Ni	$2/m..$, 4a, C_{2h}^x		1		2		2	1
P	$m2m$, 4c, C_{2v}^y	1		1	1	1	1	1

Librations of PO_4: 6 modes		
T_d	site C_{2v}^y	correlation to D_{2h}
T_1	$A_2 + B_1 + B_2$	$A_u + B_{1g} + B_{1u} + B_{2g} + B_{3g} + B_{3u}$

Internal modes of PO_4: 18 modes		
T_d	site C_{2v}^y	correlation to D_{2h}
ν_1 (A_1)	A_1	$A_g + B_{2u}$
ν_2 (E)	$A_1 + A_2$	$A_g + B_{2u} + A_u + B_{2g}$
ν_3 (T_2)	$A_1 + B_1 + B_2$	$A_g + B_{2u} + B_{1u} + B_{3g} + B_{1g} + B_{3u}$
ν_4 (T_2)	$A_1 + B_1 + B_2$	$A_g + B_{2u} + B_{1u} + B_{3g} + B_{1g} + B_{3u}$

Table 7. Assignment of the Experimental Bands of the Raman Spectra of Olivine and β'-$LiNiPO_4$

Raman shifts (cm^{-1}) $^7LiNiPO_4$	Raman shifts (cm^{-1}) $^6LiNiPO_4$	mode attribution (olivine phase)
118.3	119.4	phonon or PO_4 libration
168.8	169.6	phonon or PO_4 libration
174.3	175.3	phonon or PO_4 libration
236.3	238.5	phonon or PO_4 libration
256.6	257.5	phonon or PO_4 libration
280.5	283	phonon or PO_4 libration
301.7	304	phonon or PO_4 libration
322.3	323.5	phonon or PO_4 libration
416.8	417	ν_2
437.8	439	ν_2
466	467.8	ν_2
582.7	580.7	ν_4
590.9	591	ν_4
600	601	ν_4
640	641.4	ν_4
947.5	948.5	ν_1
1010	1011	ν_3
1021		double phonon or ν_3
1071	1072.5	ν_3
1086	1088	ν_3

Raman shifts (cm^{-1}) $^7LiNiPO_4$	Raman shifts (cm^{-1}) $^6LiNiPO_4$	mode attribution (β' phase)
185	189.4	phonon or PO_4 libration + lithium
251.1	250.5	phonon or PO_4 libration
258.5	256.5	phonon or PO_4 libration
342	364.8	lithium
455	453.5	ν_2
497.5	522	lithium
565.4	565	ν_4
622	625	ν_4
648.7	654	ν_4 + lithium
912.8	913	double phonon or ν_3
940.5	939.4	ν_1
1057.8	1058	ν_3
1149.7	1148	ν_3

With the help of Tables 5 and 6, the experimental bands can be assigned to specific vibrations. This is done in Table 7 for both phases of $LiNiPO_4$.

We shall first comment on the olivine phase data.

In the region where internal modes of the phosphate anion appear, we identify the totally symmetric mode at ν_1 = 947.5 cm^{-1}; the doublet ν_2 between 416 cm^{-1} and 466 cm^{-1}; and the triplets ν_3 and ν_4 in the regions 1010−1086 cm^{-1} and 580−640 cm^{-1}, respectively. As expected, internal bands are split because of site-symmetry and correlation effects. From these two factors, the former is expected to be dominant because the PO_4 tetrahedron is considerably distorted. However, the appearance of more than two peaks in the ν_2 region and more than three in the ν_4 region can only be due to correlation effects, as these frequencies are too high to be due to Ni or PO_4 translations. The weak shoulder at 1020 cm^{-1} might be ascribed to a second-order peak.

Below 400 cm^{-1}, we expect the 12 translational modes of Ni and PO_4, plus 6 librations of PO_4 (only 3 if we neglect correlation effects). In any case, we expect more modes than are observed. There are some possible explanations for this discrepancy: some of the missing modes might be at frequencies below 100 cm^{-1} or unresolved in the experimental spectrum, or their Raman activity is just be too low to be detected. Modes of PO_4 as whole, for instance, are likely to be unobserved.

The mode attribution in this region might be done more accurately by measuring the temperature evolution of the spectrum or by partial substitution of Ni or PO_4 by other transition metals or tetrahedral anions, respectively.

Substitution of ^7Li by ^6Li in the olivine phase of $LiNiPO_4$ does not result in any remarkable change in the Raman spectrum. The differences observed between the Raman shifts in $^6LiNiPO_4$ and in $^7LiNiPO_4$ are within the experimental error. This agrees with the fact that lithium is not Raman-active in this phase.

In the β' phase, we expect only 6 translational modes (3 from Li and 3 from PO_4), 3 librational modes, and 9 internal modes. In this phase, there is no extra splitting of Raman bands by correlation effects, and in fact, the number of peaks appearing in the internal-mode region can be explained by the low-symmetry site of the PO_4 anion. As in the olivine phase, we attribute the peak at 913 cm^{-1} in the β' phase to second-order activity, because its frequency is quite low to be a component of ν_3 and no correlation splitting of ν_1 is expected. Moreover, this agrees with twice the ν_2 value. If this attribution is correct, then the splitting of the degenerate internal modes is lower than predicted by symmetry: the triplet modes split into a singlet and a doublet, and the ν_2 doublet does not split. This suggests that the actual symmetry of the PO_4 group might be higher than C_{2v} or close to a higher symmetry group.

The assignment given in Table 7 is based on the same arguments as for the olivine phase. In the β' phase, the availability of samples synthesized with the ^6Li isotope has been used to ascribe the bands at 342 and 497 cm^{-1} to lithium-only vibrations, as the relation between these values and the corresponding ones in the ^6Li compound (365 and 522 cm^{-1}, respectively) is very close to the inverse-square-root-of-the-masses law. There are two other modes, at 185 and 648 cm^{-1}, whose frequencies also increase with ^6Li substitution (to 189 and 654 cm^{-1}, respectively). Therefore, we attribute to them a mixed character, of translational plus librational type, for the 185 cm^{-1} mode, and of translational plus internal type, for the 648 cm^{-1} mode. As in the olivine phase, we detect fewer modes than expected in the low-frequency region.

The detection of modes due to lithium translation confirms the structural hypothesis, in particular the modification in the lithium coordination from 6- to 4-fold upon synthesis under pressure. On the other hand, the detection of well-defined modes associated with lithium suggests that the lithium sublattice is static, at least at room temperature, which agrees with the conductivity results.

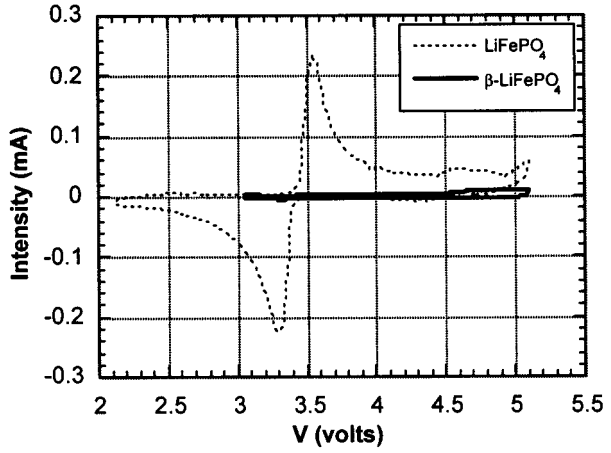

Figure 10. Electrochemical performance of olivine and β'-LiFe4PO_4.

Finally, we comment on the apparent lack of correlation between the experimental frequencies of the ν_1 mode in the olivine and β' phases (947 and 940 cm^{-1}, respectively) and the length of the P−O bonds. Usually, the shorter bonds of the β' phase should result in higher stretching frequencies. We might find the explanation, however, in the different coordination of the PO_4 tetrahedra in the two phases: in the olivine phase, the P−O stretching vibration alsoinvolves, to a high degree, the stretching of Ni−O bonds, whereas in the β' phase, the ν_1 mode involves, together with the P−O stretching, the bending of the O−Ni−O angles.

Electrochemical Behavior. The effect of the olivine ⇔ β'-$LiMPO_4$ phase transition on the electrochemical properties of these materials is clearly observed in Figure 10. As previously reported,[7] among the $LiMPO_4$ (M = Mn, Fe, Ni) olivines, only the iron-containing compound is electrochemically active within the stability window of the electrolyte (from 0.0 to 5.1 V). From the olivine $LiFePO_4$, up to 0.8 lithium per unit formula can be reversibly extracted at about 3.7 V, whereas no oxidation results for the β'-$LiMPO_4$ materials. In this connection, the $LiCoPO_4$ olivine has very recently been reported to be a very promising high-voltage cathodic material.[8]

It is well-known that an electrochemical cell transforms chemical energy into electrical energy. It consists of a material at the anode that is the reductant of the chemical reaction and an oxidant at the cathode. Both the reductant and the oxidant are consumed on discharge of the battery and produced on charge. The energy of their reaction divided by the electronic charge produced in the reaction gives the maximum discharge voltage of the cell. It must be recalled that raising the energy of a given redox couple in a cathode lowers the voltage of the cells using a common anode, whereas raising the redox energy of an anode raises the cell voltage for a given cathode. Because the energy of a given redox couple depends on the electrostatic field at the cation position and the covalent contribution to the cation−anion bonding,[7] the different behavior observed in the iron-containing compounds (olivine and β' phase) can be explained by the change in the value of the electrostatic field at the iron position produced by the phase transition. A Madelung calculation yields the values shown in Table 8. Thus, as a consequence of the phase transition, a significant stabilization is produced in the redox energy of the couple Fe^{3+}/Fe^{2+}, from −27.5 eV in the olivine phase to −26.7 eV in β'-$LiFePO_4$. Therefore, a significant increase of the cell voltage is expected.[7] Indeed, no electrochemical processes appear on charging β'-$LiFePO_4$ up to the upper limit of the experimental setup.

Table 8. Electrostatic Field at the Atoms Positions in Olivine and β'-$LiFePO_4$

$LiFePO_4$ olivine		β'-$LiFePO_4$	
atom	electrostatic field (V)	atom	electrostatic field (V)
Fe	−27.3	Fe	−26.7
Li	−14.9	Li	−15.3
P	−53.1	P	−59.6
O(1)	16.9	O(1)	28.7
O(2)	27.8	O(2)	27.4
O(3)	27.4		

In addition to these considerations, lithium mobility in the two structures must be considered, as high lithium mobility might favor good electrochemical performance. Because the lithium ions in the olivine structure are located in octahedral sites sharing edges, whereas in β'-$LiFePO_4$ they are in isolated tetrahedral positions, the lithium mobility in the former structure is expected to be much higher than that in the latter. However, the measured conductivity of $LiNiPO_4$ olivine is very low, above 722 K, the resistance of the pellet is too high to obtain accurate data. Thus, the ionic conductivity of $LiNiPO_4$ olivine at 772 K is as low as 10^{-8} Ω^{-1} cm^{-1}. On the other hand, the resistance of the pellet of β'-$LiNiPO_4$ is too high to be measured with the experimental setup; also, because the β'-phase transforms at room pressure to the olivine phase at about 697 K, it was not possible to determine the mobility of lithium in this material.

Conclusions

Olivine-like phosphates $LiMPO_4$ (M = Fe and Ni) undergo a phase transition under high pressure, whereas the manganese-containing compound seems to be stable, at least up to 65 kbar. Instead of the well-known olivine ⇔ spinel transition, a transformation into a new phase is produced (β' phase). The main difference between the two structures is the oxygen arrangement, as the metallic frameworks are similar. Surprisingly, the coordination of lithium is modified from 6- (in olivine) to 4-fold (in β') under pressure. The structural model proposed for the β' phase has been confirmed by Raman spectroscopy.

Among the olivines $LiMPO_4$ (M = Mn, Ni, and Fe), only the iron-containing one is electrochemically active within the electrolyte stability window (up to 5.1 V), whereas none of the high-pressure materials is active. This can be explained by the change in the electrostatic field at the transition metal position induced by the phase transition.

Acknowledgment. This study was financially supported by CICYT (Project MAT 98-1053-C04-04), CAM (Project CAM-07N/0012/1998), and USP (Project USP USP-7/99).

CM000596P